


# Heredity of clusters in the rapidly cooling processes of Al-doped $Zr_{50}Cu_{50}$ melts and its correlation with the glass-forming ability

Dadong Wen(文大东), Yonghe Deng(邓永和), Ming Gao(高明), and Zean Tian(田泽安)
**Citation:**Chin. Phys. B, 2021, 30 (**7**): 076101. DOI: 10.1088/1674-1056/abea93
Journal homepage: http://cpb.iphy.ac.cn; http://iopscience.iop.org/cpb

**What follows is a list of articles you may be interested in**

---

## A novel two-dimensional SiO sheet with high-stability, strain tunable electronic structure, and excellent mechanical properties

Shijie Liu(刘世杰) and Hui Du(杜慧)
Chin. Phys. B, 2021, 30 (**7**): 076104. DOI: 10.1088/1674-1056/abf34d

## Non-monotonic temperature evolution of nonlocal structure-dynamics correlation in CuZr glass-forming liquids

W J Jiang(江文杰) and M Z Li(李茂枝)†
Chin. Phys. B, 2021, 30 (**7**): 076102. DOI: 10.1088/1674-1056/abf113

## *Ab initio* molecular dynamics study on the local structures in $Ce_{70}Al_{30}$ and $La_{70}Al_{30}$ metallic glasses

F X Li(李福祥), J B Kong(孔吉波), M Z Li(李茂枝)
Chin. Phys. B, 2018, 27 (**5**): 056102. DOI: 10.1088/1674-1056/27/5/056102

## Five-fold local symmetry in metallic liquids and glasses

M Z Li(李茂枝), H L Peng(彭海龙), Y C Hu(胡远超), F X Li(李福祥), H P Zhang(张华平), W H Wang(汪卫华)
Chin. Phys. B, 2017, 26 (**1**): 016104. DOI: 10.1088/1674-1056/26/1/016104

## Effect of icosahedral clusters on *β*-relaxations in metallic glasses

X Q Gao(高选乔), Y T Sun(孙奕韬), Z Wang(王峥), M Z Li(李茂枝), H Y Bai(白海洋)
Chin. Phys. B, 2017, 26 (**1**): 016101. DOI: 10.1088/1674-1056/26/1/016101

---

# Heredity of clusters in the rapidly cooling processes of Al-doped $Zr_{50}Cu_{50}$ melts and its correlation with the glass-forming ability*

Dadong Wen(文大东)[1,†], Yonghe Deng(邓永和)[1], Ming Gao(高明)[1], and Zean Tian(田泽安)[2]

[1] School of Computational Science & Electronics, Hunan Institute of Engineering, Xiangtan 411104, China
[2] School of Materials Science and Engineering, Hunan University, Changsha 410081, China

(Received 29 December 2020; revised manuscript received 9 February 2021; accepted manuscript online 1 March 2021)

The heredity of clusters in rapidly cooled $(Zr_{50}Cu_{50})_{100-x}Al_x$ melts and its correlation with glass-forming ability (GFA) are studied via molecular dynamics simulations. Pair distribution function and the largest standard cluster (LSC) are adopted to characterize the local atomic structures in the $(Zr_{50}Cu_{50})_{100-x}Al_x$ systems. The [12/555] icosahedra and their medium-range order (IMRO) play an important role in forming $(Zr_{50}Cu_{50})_{100-x}Al_x$ metallic glasses (MGs). The fraction of [12/555], the number of IMRO, and the maximum size of IMRO in MGs increase significantly with increasing $x$. A tracking study further reveals that the configuration heredity of icosahedral clusters starts from supercooled liquids. No direct correlation exists between the GFA and the onset temperature of continuous or stated heredity. Instead, a larger hereditary supercooled degree of icosahedra matches with better GFA of Al-doped $Zr_{50}Cu_{50}$ alloys.

**Keywords:** glass forming ability, atomic structure, heredity, molecular dynamics

**PACS:** 61.25.Mv, 61.50.Ks, 87.15.nt **DOI:** 10.1088/1674-1056/abea93

## 1. Introduction

Bulk metallic glasses (BMGs) have attracted much attention over the past decades[1] due to their superior physical, mechanical, and chemical properties.[2,3] Considering the limitations in information regarding glass transition and glass forming ability (GFA), designing new and desirable BMGs in material science and engineering is still challenging.[2] BMGs are usually synthesized by three or more elements, and their GFA sensitively depends on the stoichiometric composition of alloys.[4] Researchers have improved the GFA and developed new BMGs by adding small amounts of alloying element(s) starting from the best binary glass-forming alloys.[5–8] For example, Figueroa *et al.*[9] found that the GFA of $Cu_{55}Hf_{45}$ alloys could be maximized with the addition of 2.0-at.% Si, and that the supercooled liquid region was increased by 15 K relative to the matrix alloy. Cai *et al.*[6] revealed that the substitution of Zr in $Cu_{50}Zr_{50}$ alloy by Al could remarkably increase the GFA, and the best glass-forming alloy was $Cu_{50}Zr_{47}Al_3$. The increase in GFA via minor doping has been explained using methods involving thermodynamics (*e.g.*, thermal stability)[9,10] and kinetics (*e.g.*, dynamic slowing down).[11] However, the atomic structural mechanism of the GFA of element-doped liquid alloys remains poorly understood because of experimental limitations.[5] Therefore, the effect of element doping on the formation and evolution of atomic configurations during rapid solidification and their correlation with the GFA need to be investigated.

Zr–Cu binary alloy is an ideal model matrix alloy for studying the effect of element doping on the formation of atomic structures and its correlation with GFA.[12–15] For example, using molecular dynamics (MD) simulations, Cheng *et al.*[16] found that adding a few at.% of Al into Zr–Cu can significantly increase the number of Cu (and Al)-centered perfect icosahedra and their medium-range orders (MROs). The increase in GFA by Al doping is attributed to the improvement of the symmetry and spatial connectivity of icosahedra via bond shortening.[17] Our previous MD simulations demonstrated that the GFA of binary glassy alloys is closely related to the configuration heredity of clusters, especially icosahedra.[18] Whether the criterion that a high hereditary ability of clusters corresponding to good GFA is applicable to the element doping is unknown. In the present work, the best glass former, $Zr_{50}Cu_{50}$, is selected as the matrix alloy for studying the correlation of the heredity of clusters with GFA of the Al-doped $Zr_{50}Cu_{50}$ alloy by MD simulation. The pair distribution function (PDF), largest standard cluster (LSC),[19] and hereditary tracking are used to characterize and analyze the atomic structures of MGs.[20] Finally, the relationship between the heredity of clusters and the GFA of $(Zr_{50}Cu_{50})_{100-x}Al_x$ alloys is established.

## 2. Simulation details

MD simulations were conducted to study the rapid solidification of $(Zr_{50}Cu_{50})_{100-x}Al_x$ ($x = 0$, 4, 8, 12, 16, 20 at.%) by using the open source code of LAMMPS.[21] A realistic interatomic potential with an embedded atom model (EAM)

*Project supported by the National Natural Science Foundation of China (Grant No. 51701071), the Natural Science Foundation of Hunan Province, China (Grant Nos. 2018JJ3100 and 2018JJ2078), and the Project of the Hunan Educational Department, China (Grant No. 19B122).

†Corresponding author. E-mail: ddwen@hnu.edu.cn

© 2021 Chinese Physical Society and IOP Publishing Ltd 

formalism was used. The potential was developed and highly optimized by Sheng *et al.*[17] The accuracy and validation of this EAM potential for Zr–Cu(–Al) were confirmed in another study.[12] MD simulations can correctly predict the structural and thermodynamic properties of liquid and solid Zr–Cu(–Al) by using this potential.[17] Subject to the three-dimensional (3D) periodic, the system was initialized as a cubic box composed of $5\times10^4$ atoms, in which Zr, Cu, and Al atoms were randomly distributed according to the stoichiometry. The MD time step was set to 2.0 fs. After the initial melting of $(Zr_{50}Cu_{50})_{100-x}Al_x$ and equilibration for 2.0 ns at 2000 K, which is considerably above the experimental liquid temperatures,[7] the system was quenched to 300 K at a cooling rate of $5\times10^{10}$ K·s$^{-1}$. The equilibrated time of 2 ns at 2000 K is long enough for the system to reach equilibrium, so that all the configurations obtained subsequently are independent of the initial structures.[17] All the simulations were performed under NPT (constant number of atoms, pressure and temperature) ensemble. The external pressure was kept at 0 Pa. The temperature was controlled using a Nose–Hoover thermostat.[22] The Andersen method[23] was applied to control pressure in every direction. During quenching, the temperature dependence of velocities and the positions of each atom were recorded at every 10 K to calculate the structural quantities.

## 3. Results and discussion

### 3.1. Evolution of potential energy

The temperature ($T$) dependence of potential energy (PE) is typically used to monitor the phase formation of liquid metals during rapid cooling[24] or melting. Figure 1 displays the PE–$T$ curves of the $(Zr_{50}Cu_{50})_{100-x}Al_x$ ($x=0$, 4, 8, 12, 16, 20) system during rapid solidification. No jumping drop in the PE–$T$ curves can be observed, indicating that rapid cooling is related to glass transition and not first-order phase transitions, such as crystallization.[25] The PE–$T$ curves of $(Zr_{50}Cu_{50})_{100-x}Al_x$ systems decrease linearly when cooling from 2000 K to 1300 K. Such linear temperature dependence of PE can also be observed from 1200 K to 900 K but with a slightly different slope. Upon cooling from 900 K to 600 K, PE varies smoothly but deviates evidently from a linear dependence of temperature. Usually, the glass transition is believed to occur within this temperature range. The glass transition temperatures $T_g=702$, 723, 735, 752, 775, 805 K are estimated according to the departure of PE from its linear relationship with temperature from 300 K to 900 K for $x=0$, 4, 8, 12, 16, 20, respectively (see the inset of Fig. 1). The present glass transition temperature is slightly higher than that obtained in the experiment:[7] $T_g=670$, 689, 701 K for $x=0$, 4, 8, respectively. These differences may be due to the much higher cooling rates used in our MD simulations. However, the $T_g$ value in experiment for $x=12$, 16, 20 has not been reported yet. At a certain temperature the system energy increases linearly with the increase of $x$, indicating the addition of Al atoms decreases the stability of the alloys.

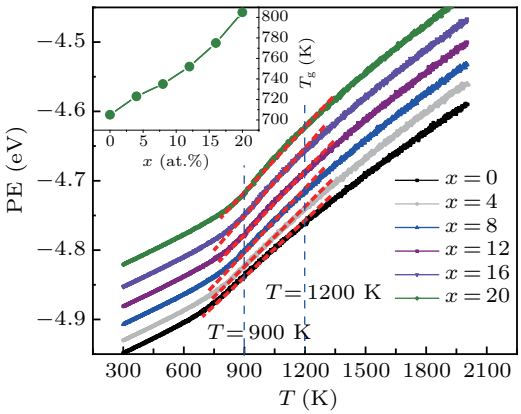



**Fig. 1.** The potential energy (PE) per atom in the $(Zr_{50}Cu_{50})_{100-x}Al_x$ systems *versus* temperature $T$ in the processes of rapid cooling. The red dashed lines denote the linear fittings. The insert is the $T_g$ at different Al concentration $x$.

### 3.2. PDF

As a one-dimensional (1D) analysis technique, the PDF g(r) has been widely used to detect the microstructural characteristics of liquid, crystal, and glass,[1] because it can be transformed into the structure factor $S(q)$ obtained from x-ray diffraction (XRD) data by Fourier transformation. The function $g(r)$ is defined as follows:

$$g(r)=\frac{V}{N^2}\left\langle\sum_{i=1}^{N}\frac{n(r)}{4\pi r^2\Delta r}\right\rangle, \tag{1}$$

where $N$ is the total number of atoms in a simulation cell, $V$ is the volume, and $n(r)$ is the number of atoms that can be found in the shell from $r$ to $r+\Delta r$. It should be noted that the $g(r)$ experimentally is obtained by Fourier transformation from $S(q)$ measured by XRD or neutron diffraction experiment, while its theoretical value is calculated directly by Eq. (1).

Figure 2(a) illustrates the $g(r)$ curves of rapidly cooling liquid $(Zr_{50}Cu_{50})_{100-x}Al_x$ (only $x=0$, 8, 20 are shown) at several selected temperatures. At the initial temperature $T=2000$ K, the $g(r)$ curve of each alloy exhibits a wide first peak and a very smooth second peak but no obvious third peak, revealing the typical feature of liquid.[26] However, the first peak of the $g(r)$ curves in $(Zr_{50}Cu_{50})_{100-x}Al_x$ systems becomes sharper, and the second peak of the $g(r)$ curves exhibits an evident shoulder with decreasing temperature. These results indicate that some short-range orders, even some MROs, emerge in the rapidly solidified solids below $T_g$ compared with other states.[27] The split-second peak and an increase in the shoulder of $g(r)$ curves indicate that the rapidly solidified $(Zr_{50}Cu_{50})_{100-x}Al_x$ ($x=0$, 8, 20) is amorphous, and the number of MROs in the rapidly solidified solids increases

with decreasing temperature.[17] Through the Fourier transformation of RDF, the structure factor $S(q)$ for the simulated $(Zr_{50}Cu_{50})_{100-x}Al_x$ ($x = 0$, 8) MGs at 300 K is obtained and depicted in Fig. 2(b) together with the experimental data.[28,29] Our MD simulation results agree well with the experimental results. Therefore, the present MD calculations are relatively accurate in simulating the rapid solidification of liquid $(Zr_{50}Cu_{50})_{100-x}Al_x$.

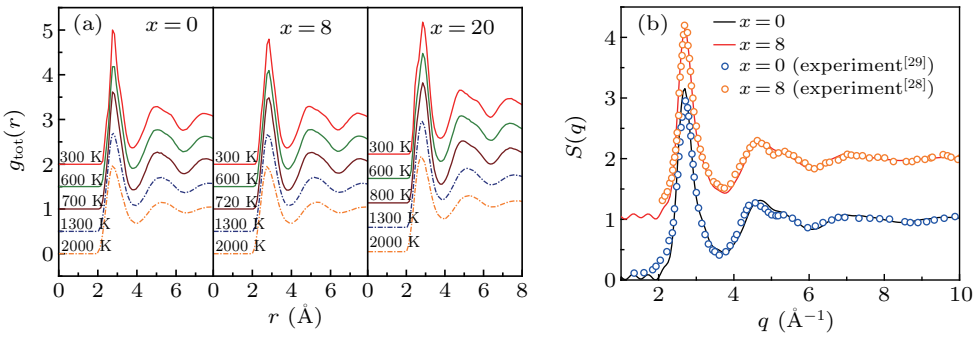



**Fig. 2.** (a) Total PDFs for the rapidly cooled $(Zr_{50}Cu_{50})_{100-x}Al_x$ alloys at several selected temperatures. (b) Comparison of $S(q)$ for $(Zr_{50}Cu_{50})_{100-x}Al_x$ MGs at 300 K between this simulation and other experiments.[28,29]

### 3.3. Coordination number

Coordination number (CN) is further adopted to provide a statistical description of atoms bounded in $(Zr_{50}Cu_{50})_{100-x}Al_x$ MGs for structural analysis. The CNs can be derived by

$$CN_{ij} = \int_0^{r_{\min}} 4\pi\rho_0 c_j r^2 g_{ij}(r)\,\mathrm{d}r, \tag{2}$$

where $\rho_0$ is the number density of atoms in the system of $N$ atoms, $c_j$ is the concentration of a $j$-th component, $r_{\min}$ denotes the position of the minimum of the first valley of $g_{ij}(r)$ curve. The total CN for atom $i$ is calculated by $CN_i = \sum CN_{ij}$.[30] Table 1 lists the total CNs for $(Zr_{50}Cu_{50})_{100-x}Al_x$ MGs at 300 K. One can see that our simulated results for $x = 0$ are in well agreement with the MD results[30] in literatures although slightly different from the experimental values.[29] The total $CN_{all}$ keeps nearly constant at 13 for $(Zr_{50}Cu_{50})_{100-x}Al_x$ alloys, while $CN_{Cu}$ and $CN_{Zr}$ increases slightly with increasing Al concentration. This indicates that Al addition can increase the packing density of local atomic structures centered by Zr or Cu atom.[17] In all systems considered in present work, the findings that $CN_{Zu}$ is the largest followed by $CN_{Al}$ and $CN_{Cu}$ may result from their different atomic Goldschmidt radii ($R_{Zr} = 1.6$ Å, $R_{Al} = 1.43$ Å, $R_{Cu} = 1.28$ Å).[30]

**Table 1.** *CN*s for $(Zr_{50}Cu_{50})_{100-x}Al_x$metallic glasses at 300 K.

| *CN* | $x = 0$ | | | $x = 8$ | $x = 20$ |
|---|---|---|---|---|---|
| | This work | Experiment[29] | MD[30] | This work | This work |
| $CN_{Zr}$ | 15.14 | 14.45 | 15.04 | 15.18 | 15.28 |
| $CN_{Cu}$ | 10.76 | 10.27 | 10.65 | 10.89 | 11.07 |
| $CN_{Al}$ | – | – | – | 11.89 | 11.76 |
| $CN_{all}$ | 12.95 | 12.36 | 12.95 | 12.95 | 13.00 |

### 3.4. LSC

The LSC analysis (LSCA)[19,20,31] is further conducted to characterize and analyze the local atomic structures of liquid $(Zr_{50}Cu_{50})_{100-x}Al_x$ ($x = 0$, 4, 8, 12, 16, 20) during rapid solidification and to obtain insights into the 3D structural details of the system. In LSCA, a cluster is defined as the basic local atomic structure consisting of one central atom and all its nearest neighboring atoms. Around a given atom, the LSC is defined as the largest cluster that satisfies a unique topological criterion. In the LSC (Fig. 3), a reference pair comprising the center and one of its neighbors, as well as the pair's common near neighbors (CNNs) constitute a common neighbor subcluster. With LSCA, all types of local clusters beyond the nearest neighbor can be characterized without depending on any preset parameters.[26] The details of the topological criterion and an implementing algorithm have been presented in another study.[19] Figure 3(a) displays a distorted icosahedron[20] LSC around atom O composed of eight S555, two S544, and two S433 with the 12 neighbors. One S555 in the LSC shown in Fig. 3(b) consists of one reference pair of O–A2 and their five CNNs labeled as A1, B1, C2, A3, and A4. One S544 in Fig. 3(b) comprises the reference pair of O–B1 and their five CNNs labeled as A1, A6, C1, C2, and A2. Thus, the compact denotations for distorted icosahedron

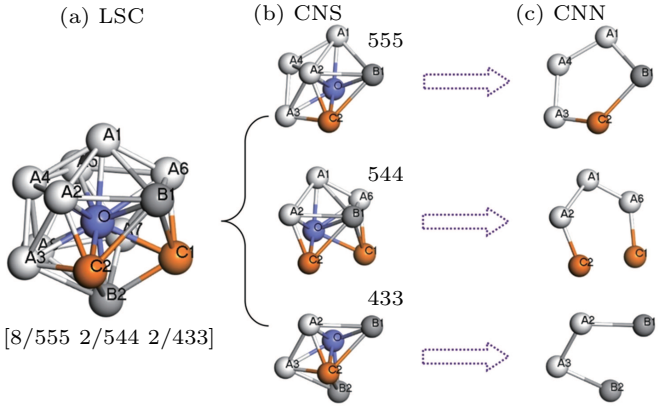



**Fig. 3.** Topology of the largest standard cluster (LSC). (a) A [8/555 2/544 2/433] distorted icosahedral cluster composed of a central atom (labeled O) and 12 neighbors; (b) the topology of three CNSs; (c) the topology of three CNNs. For example, a CNS of S555 composed of a bonded reference pair (labeled O and A2) and 5 CNNs (labeled A1, B1, C2, A3, and A4).

LSC are expressed as [8/555 2/544 2/433]. Similarly, [12/555] corresponds to a perfect icosahedron comprising 13 atoms associated with 12 S555. A defective icosahedron consisting of 14 atoms associated with one S444, ten S555, and two S666 can be expressed as [1/444 10/555 2/666].

Through the LSCA, various LSCs are identified in the rapidly cooled $(Zr_{50}Cu_{50})_{100-x}Al_x$ ($x$ = 0, 4, 8, 12, 16, 20) systems. Table 2 lists the numbers of the top 30 typical LSCs in the $(Zr_{50}Cu_{50})_{100-x}Al_x$ ($x$ = 0, 8, 20) MGs at 300 K. The LSCs have a small Cu atom as a center for the $CN < 13$, but the center is a large Zr atom when $CN > 14$ for $x = 0$, thereby agreeing well with our previous findings[32] in Zr–Cu binary MGs. Among these LSCs, the Cu-centered [12/555] icosahedra and [8/555 2/544 2/433] distorted icosahedra are dominant in terms of number, thereby showing a typical structural feature of a glassy state. As for $x$ =8, 20, the number of [12/555] icosahedra is dominant, followed by that of [8/555 2/544 2/433]. The numbers of these two LSCs are much larger than those in $Zr_{50}Cu_{50}$ MGs. When $CN < 13$, the LSCs have a Cu or Al atom at the center, whereas when $CN > 14$, the LSCs have a Zr atom at the center. An Al atom is at the center of icosahedron-type clusters, such as [12/555], [8/555 2/544 2/433], and [8/555 2/444 2/666]. Among the [12/555] icosahedra, the Al-centered ones in $(Zr_{50}Cu_{50})_{92}Al_8$ MGs account for 31.7%, thereby indicating that Al doping can promote the formation of icosahedral clusters, especially the [12/555] perfect ones in $(Zr_{50}Cu_{50})_{100-x}Al_x$ MGs.

**Table 2.** Number of various types of LSCs in $(Zr_{50}Cu_{50})_{100-x}Al_x$metallic glasses.

| *CN* | LSC index | $x = 0$ | | $x = 8$ | | | $x = 20$ | | |
|---|---|---|---|---|---|---|---|---|---|
| | | Centered by | | Centered by | | | Centered by | | |
| | | Zr | Cu | Zr | Cu | Al | Zr | Cu | Al |
| 10 | [1/444 5/555 1/544 3/433] | 0 | 355 | 0 | 461 | 8 | 0 | 378 | 18 |
| | [4/555 2/422 4/433] | 0 | 275 | 0 | 293 | 4 | 0 | 229 | 10 |
| 11 | [2/444 8/555 1/666] | 0 | 935 | 0 | 980 | 40 | 0 | 738 | 61 |
| | [1/444 6/555 2/544 2/433] | 0 | 766 | 0 | 842 | 31 | 1 | 675 | 84 |
| | [2/444 4/555 1/666 2/544 2/433] | 0 | 415 | 1 | 368 | 16 | 1 | 245 | 26 |
| | [1/444 4/555 2/422 2/544 2/433] | 0 | 396 | 0 | 285 | 17 | 0 | 230 | 4 |
| 12 | **[12/555]** | **11** | **1269** | **10** | **1351** | **632** | **13** | **2090** | **1594** |
| | [8/555 2/544 2/433] | 20 | 1262 | 10 | 1227 | 462 | 12 | 1501 | 1091 |
| | [8/555 2/444 2/666] | 6 | 1064 | 1 | 988 | 118 | 0 | 801 | 222 |
| | [2/444 4/555 2/666 2/544 2/433] | 10 | 519 | 5 | 415 | 40 | 0 | 347 | 98 |
| | [2/444 5/555 1/666 3/544 1/433] | 0 | 528 | 0 | 383 | 48 | 0 | 292 | 94 |
| | [3/444 6/555 3/666] | 1 | 421 | 0 | 393 | 30 | 0 | 292 | 49 |
| | [6/555 2/422 2/544 2/433] | 6 | 249 | 7 | 204 | 76 | 0 | 234 | 191 |
| | [5/555 1/421 3/544 3/433] | 6 | 244 | 6 | 203 | 71 | 0 | 223 | 150 |
| 13 | [3/444 6/555 4/666] | 39 | 654 | 23 | 621 | 91 | 10 | 453 | 191 |
| | [1/444 10/555 2/666] | 130 | 392 | 87 | 368 | 172 | 49 | 432 | 429 |
| 14 | [2/444 8/555 4/666] | 292 | 102 | 226 | 83 | 32 | 134 | 82 | 130 |
| | [1/444 7/555 2/666 3/544 1/433] | 397 | 14 | 305 | 8 | 18 | 212 | 17 | 37 |
| | [9/555 1/666 3/544 1/433] | 310 | 4 | 263 | 3 | 5 | 214 | 9 | 22 |
| 15 | [9/555 2/666 3/544 1/433] | 759 | 0 | 884 | 0 | 0 | 891 | 2 | 4 |
| | [1/444 10/555 4/666] | 651 | 2 | 676 | 1 | 2 | 558 | 6 | 8 |
| | [1/444 7/555 3/666 3/544 1/433] | 604 | 1 | 590 | 1 | 1 | 454 | 1 | 14 |
| | [12/555 3/666] | 384 | 0 | 480 | 0 | 0 | 465 | 3 | 1 |
| | [2/444 8/555 5/666] | 457 | 4 | 409 | 6 | 3 | 312 | 3 | 13 |
| | [6/555 1/666 6/544 2/433] | 344 | 0 | 346 | 0 | 0 | 320 | 2 | 0 |
| 16 | [1/444 10/555 5/666] | 463 | 0 | 668 | 0 | 0 | 714 | 0 | 1 |
| | [12/555 4/666] | 275 | 0 | 473 | 0 | 0 | 727 | 0 | 0 |
| | [9/555 3/666 3/544 1/433] | 257 | 0 | 418 | 0 | 0 | 510 | 0 | 0 |
| | [2/444 8/555 6/666] | 236 | 0 | 288 | 0 | 0 | 273 | 0 | 0 |
| | [1/444 7/555 4/666 3/544 1/431] | 210 | 0 | 277 | 1 | 0 | 268 | 0 | 1 |
| | **Sum** | **5868** | **9871** | **6453** | **9485** | **1917** | **6138** | **9285** | **4579** |

Figure 4 plots the temperature dependence of the fraction $f_{\rm LSC}$ (*i.e.*, the ratio of the cluster number to the total number of the atoms in the simulation box) among the top five LSCs in Table 2. Each $f_{\rm LSC}$ is very small (< 0.2%) in the initial liquids of $(Zr_{50}Cu_{50})_{100-x}Al_x$ ($x$ = 0, 8, 20) and changes gradually at temperatures higher than 1000 K. With decreasing temperature, each $f_{\rm LSC}$ increases, especially for [12/555] perfect icosahedra and [8/555 2/544 2/433] distorted icosahedra. In the $Zr_{50}Cu_{50}$ alloy, the $f_{\rm LSC}$ of [12/555] increases from 0.6% to 2.2% with decreasing temperature from 1000 K to $T_{\rm g}$.

By contrast, in the $(Zr_{50}Cu_{50})_{92}Al_8$ alloy, the increase reaches 2.8%, which is larger than that of any other LSCs. These findings indicate that Al doping favors the formation of icosahedral clusters in $(Zr_{50}Cu_{50})_{100-x}Al_x$ alloys, especially in supercooled liquids and MGs, thereby promoting the formation of $(Zr_{50}Cu_{50})_{100-x}Al_x$ MGs.

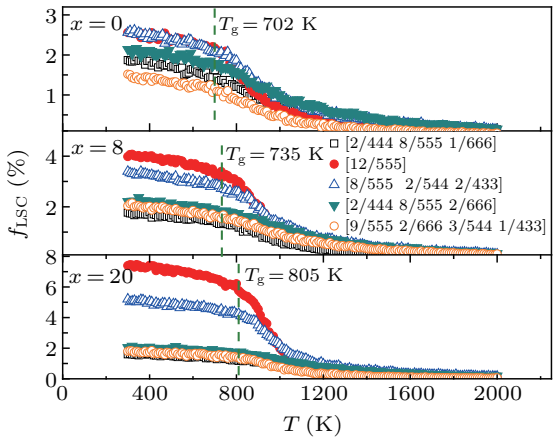



**Fig. 4.** The temperature dependence of the fraction, $f_{LSC}$, of five typical LSCs during the rapid cooling processes of liquid $(Zr_{50}Cu_{50})_{100-x}Al_x$.

### 3.5. MROs

Various LSCs are not isolated from each other but linked by vertex sharing (VS), edge-sharing (ES), face-sharing (FS), or intercross-sharing (IS) atoms, as shown in Fig. 5(a). In this case, some extended clusters, even MROs, are formed. However, not all extended clusters can be considered MROs in simulated systems. In the present work, only extended clusters associated with IS-linkage, *i.e.*, those whose central atoms are bonded with one another are considered MROs. In view of the key role of icosahedral clusters in the formation of $(Zr_{50}Cu_{50})_{100-x}Al_x$ MGs, the icosahedral MROs (IMROs),[32] which are the extended clusters consisting of [12/555] LSCs by IS-linkage, are only considered to examine the effect of Al doping on the atomic structures beyond the nearest neighbors. As in many binary glassy alloys (*e.g.* Cu–Zr[18]), even some long string-like IMRO backbones such as the interpenetration networks of IS-linkages can be observed, as shown in Figs. 5(b) and 5(c).

Figure 6 shows the number of IMRO ($N_{IMRO}$) and the maximum size of IMROs ($n_{max}$) in rapidly cooled $(Zr_{50}Cu_{50})_{100-x}Al_x$ glassy alloys at 300 K. Similar to [12/555] LSCs, $N_{IMRO}$ and $n_{max}$ increase significantly with increasing Al concentration $x$, indicating that the order degree and the packing density of local atomic structures in $(Zr_{50}Cu_{50})_{100-x}Al_x$ MGs are significantly improved by the increase in Al concentration. These findings may be due to the bond shortening induced by Al doping in the system.[16,17] However, these findings do not mean that the GFA of $(Zr_{50}Cu_{50})_{100-x}Al_x$ alloys is monotonously improved with increasing $x$.[7] In our previous work,[32] we showed that the hereditary characters instead of the number or fraction of the icosahedral clusters are correlated intimately with the GFA of glassy alloys. Hence, the heredity of icosahedral clusters in the rapid cooling processes of $(Zr_{50}Cu_{50})_{100-x}Al_x$ alloys is further examined in the following section.

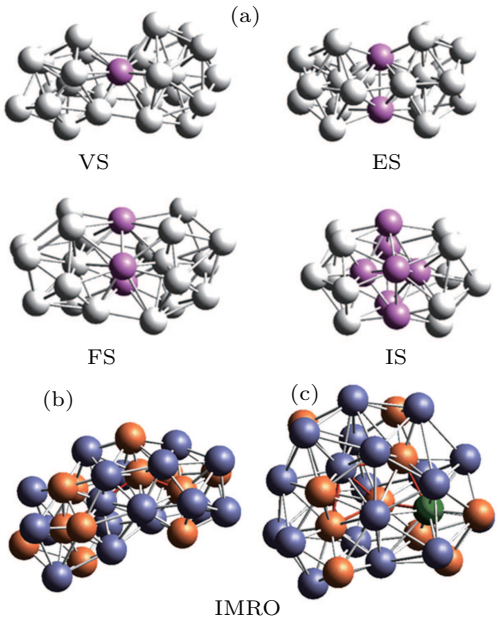



**Fig. 5.** Schematic diagram of extended clusters and typical IMRO structures. (a) VS, ES, FS, and IS linkages between two icosahedra (The pink balls represent shared atoms); (b) A small IMRO combined by four [12/555] in $Zr_{50}Cu_{50}$ MG; (c) A small IMRO composed of six [12/555] icosahedra in $(Zr_{50}Cu_{50})_{92}Al_8$ MG. The slateblue, orange, and green balls represent Zr, Cu, and Al atoms, respectively.

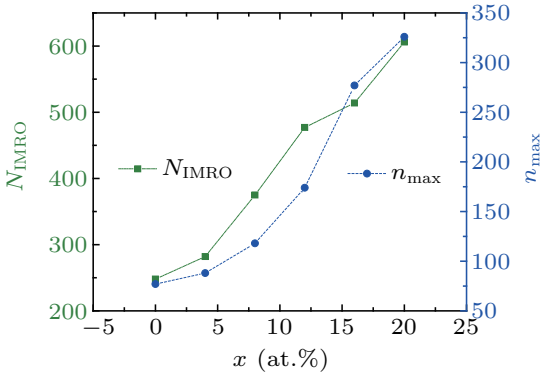



**Fig. 6.** The number $N_{IMRO}$ and the max size $n_{max}$ of IMROs in rapidly cooled $(Zr_{50}Cu_{50})_{100-x}Al_x$ glassy alloys at 300 K.

### 3.6. Heredity of icosahedra and its correlation with the GFA

To understand the relationship between local atomic structures and the GFA of $(Zr_{50}Cu_{50})_{100-x}Al_x$ ($x = 0$, 4, 8, 12, 16, 20) alloys, the hereditary characters of icosahedral clusters are further examined by using an inverse tracking method of atom trajectories. According to previous studies,[18,32] as an LSC is being transformed to another one with the same central atom from high temperature to low temperature, the evolution is designated as a perfect heredity if the type of LSC index and the IDs of the central atom and its nearest neighbors remain unchanged. If only the LSC index and IDs of

the core atom and a part of the surrounding atoms remain unchanged, then the transformation is designated as a core heredity. Either perfect or core heredity is the configuration heredity of LSCs, which can be further classified into staged and continuous heredity in terms of inheritance duration.[20] The former denotes that the geometrical configuration of LSCs is merely kept in a narrow temperature range, whereas the latter indicates that the LSC can be uninterruptedly detected at gradually increasing temperatures, because it is identified at a low temperature, *e.g.*, 300 K. The highest temperature is defined as the onset temperature of LSCs, $T_{\rm onset}$, from which at least one of LSCs can be directly passed down to the final sate of rapidly solidified alloys.[18,20] As an example, figure 7(a) illustrates the heredity and evolution of [12/555] LSC centered by No. 28040 Cu atom in the rapid solidification of $(Zr_{50}Cu_{50})_{92}Al_8$ alloys. This LSC at 300 K can be traced back to an [12/555] icosahedron at 900 K. The onset of heredity of the [12/555] LSC with a No. 28040 atom at the center occurs in the supercooled liquid region of rapidly solidified $(Zr_{50}Cu_{50})_{92}Al_8$ alloys, and 900 K can be regarded as its $T_{\rm onset}$.[18] Based on this viewpoint, the heredity of some IMROs[32] can also be observed. Examples include the growth of IMRO consisting of No. 38178 and No. 46934 cores from $N_{\rm I}=2$ and $n=19$ to $N_{\rm I}=4$ and $n=31$, as shown in Fig. 7(b), where $N_{\rm I}$ and $n$ respectively represents the number of core atoms and the total number of atoms in an IMRO. Similar to the LSC centered by No. 28040 atom, the IS-linkage[32] between No. 38178 and No. 46934 atoms has remained unchanged, because the IMRO with $N_{\rm I}=2$ and $n=19$ emerges at 780 K. Therefore, the temperature of 780 K can also be regarded as the $T_{\rm onset}$ of descendible IMRO with $N_{\rm I}=4$ and $n=31$. In the present work, the hereditary characters of IMROs are very similar to those of [12/555] LSCs.[32] Hence, we focus on the hereditary characters of [12/555] LSCs.

A careful analysis reveals that no largest standard cluster in $(Zr_{50}Cu_{50})_{100-x}Al_x$ ($x=4$, 8, 12, 16, 20) MGs at 300 K comes from the initial melts. For most of the LSCs listed in Table 2, only a few can be traced back to the supercooled liquid. For example, only 5 of 1993 [12/555] perfect icosahedra in $(Zr_{50}Cu_{50})_{92}Al_8$ MGs at 300 K can be tracked gradually until $T_{\rm onset}=900$ K. Compared with the [8/555 2/544 2/433] and [2/444 8/555 2/666] distorted icosahedra, [12/555] perfect icosahedra in $(Zr_{50}Cu_{50})_{100-x}Al_x$ alloys possess the highest $T_{\rm onset}$. For $x=0$, 4, 8, 12, 16, 20, the $T_{\rm onset}$ of [12/555] LSC in $(Zr_{50}Cu_{50})_{100-x}Al_x$ alloys is estimated to be 770, 850, 900, 910, 920, and 930 K, respectively. This monotonous increase of the $T_{\rm onset}$ with increasing $x$ indicates that Al doping can improve the continuous heredity of [12/555] perfect icosahedra. However, the onset heredity of [12/555] LSCs still emerges in the supercooled liquids of Al-doped $Zr_{50}Cu_{50}$ alloys,[16] similar to the findings for some binary alloys, such as Zr–Cu[32] and Pd–Si.[20]

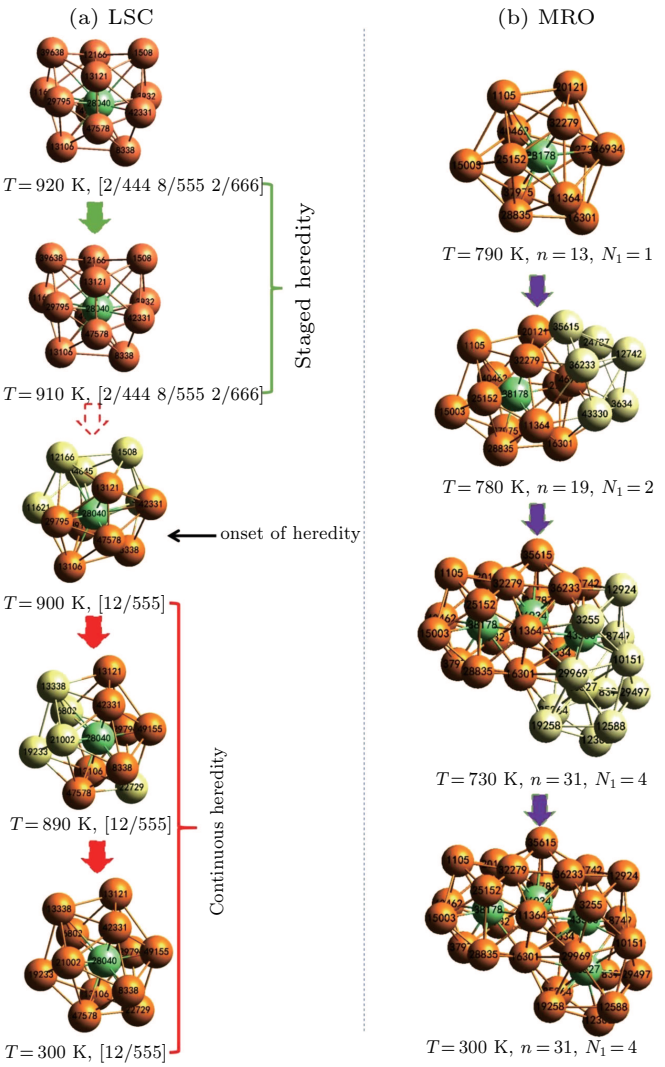



**Fig. 7.** Schematic diagram of evolution and heredity for [12/555] LSC and a typical IMRO in the rapid solidification of $(Zr_{50}Cu_{50})_{92}Al_8$ alloys. Orange and light-green balls denote the heritable shell atoms and core atoms in the IMRO, respectively. The light-yellow balls stand for the newly added core and shell atoms in the heredity of icosahedral clusters.

Furthermore, the temperature dependence of the fraction $f_{\rm S}$ of staged heredity[18] of [12/555] LSCs in $(Cu_{50}Zr_{50})_{100-x}Al_x$ alloys is investigated. In the present work, the $f_{\rm S}$ is defined as follows:

$$f_{\rm S}(T)=\frac{N_{\rm h}(T)}{N(T)}\times 100\%, \tag{3}$$

where $N_{\rm h}(T)$ is the number of icosahedra that can be passed down by staged heredity from $T$ to $T$–$\Delta T$ (herein, $\Delta T=20$ K) $N(T)$ is the total number of icosahedra at $T$. A representative data set is illustrated in Fig. 8(a). The $f_{\rm S}$ is almost zero at above 920 K and increases rapidly with decreasing $T$ below 900 K, especially in the temperature range of $T_{\rm onset}$–$T_{\rm g}$. Similar to continuous heredity, the staged heredity of [12/555] LSCs also starts from supercooled liquids, and its initial temperature $T_{\rm init}$ ($\approx 910$ K for $x=8$) is slightly higher than the $T_{\rm onset}$ ($\approx 900$ K for $x=8$). The correlation of the $T_{\rm init}$ with

the Al content $x$ is plotted in Fig. 8(b). The $T_{\rm init}$ ascends monotonously from 780 K to 940 K with $x$ changes from 0 to 20, implying that Al doping can significantly enhance the staged heredity of [12/555] LSCs in supercooled liquids. A characteristic transition temperature $T_{\rm s}$ in the curve of $f_{\rm s}$ *versus* $T$ is deduced in terms of $\partial f_{\rm s}/\partial T$, as shown in Fig. 8(a). Similar to the $T_{\rm init}$, the $T_{\rm s}$ also increases with increasing Al content $x$, as shown in Fig. 8(b). However, neither $T_{\rm init}$ nor $T_{\rm s}$ is directly correlated with the GFA of Al-doped $Zr_{50}Cu_{50}$ alloys, because the best GFA for $(Zr_{50}Cu_{50})_{100-x}Al_x$ alloys is at $x = 8$ according to the results of experiments.[7]

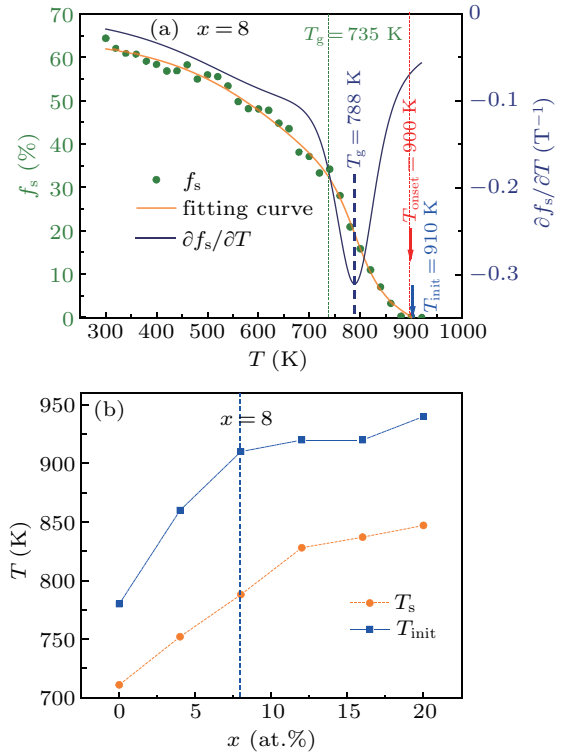



**Fig. 8.** (a) The staged hereditary fraction $f_{\rm s}$ of [12/555] icosahedra as a function of temperature during the rapid solidifications of liquid $(Zr_{50}Cu_{50})_{92}Al_8$. (b) Al content $x$ dependence of the initial temperature $T_{\rm init}$ of staged heredity and transition temperature $T_{\rm s}$ of $f_{\rm s}$.

We have demonstrated that the supercooled degree $\Delta T_{\rm S} = T_{\rm onset} - T_{\rm s}$ of continuous heredity is a good indicator for the assessment of the GFA of Zr–Cu binary alloys.[32] Hence, the hereditary supercooled degree for both continuous and staged heredity of [12/555] LSCs is investigated to establish the relationship between the local atomic structures and the GFA of $(Zr_{50}Cu_{50})_{100-x}Al_x$. In the present work, the supercooled degree for staged heredity is defined as $\Delta T_{\rm I} = T_{\rm init} - T_{\rm s}$. Figure 9(a) displays the correlation of the hereditary supercooled degree $\Delta T$ with the Al content $x$. The trend of either $\Delta T_{\rm S}$ or $\Delta T_{\rm I}$ with $x$ is highly consistent with the $x$ dependence of the diameter $D$ in the experiment,[7] especially for $0 \le x \le 12$. This finding clearly shows that the hereditary supercooled degree of [12/555] icosahedra is directly correlated with the GFA of Al-doped $Zr_{50}Cu_{50}$ alloys. The better the GFA is, the larger the $\Delta T_{\rm I}$ or $\Delta T_{\rm S}$ is. The $\Delta T_{\rm I}$ can also be used as an indicator to assess the GFA of $(Zr_{50}Cu_{50})_{100-x}Al_x$ ($\le x \le 20$) as $\Delta T_{\rm S}$.[32] Hence, a good GFA of Al-doped $Zr_{50}Cu_{50}$ alloy is attributed to the large hereditary supercooled degree of icosahedra. To gain deep insight into the correlation of the GFA with the hereditary characterizers of [12/555] LSCs, figure 9(b) further plots the correlation of the dimensionless parameter $H_{\rm i} = (T_{\rm i} - T_{\rm s})/T_{\rm s}$ with the Al content $x$, in which $i$ = ini and onset. Interestingly, the alloy composition with a bigger $H_{\rm i}$ parameter tends to have a better GFA, especially for $H_{\rm ini}$. That is, $H_{\rm i}$ parameter could also be regarded as an index to evaluate the GFA of $(Zr_{50}Cu_{50})_{100-x}Al_x$ ($0 \le x \le 20$) alloys, similar to the hereditary supercooled degree $\Delta T$. Therefore, we concluded that the heredity of local atomic configurations is the indeed an inherent property of rapid solidified alloys, and the heritability of clusters can be used to estimate the GFA of liquid $(Zr_{50}Cu_{50})_{100-x}Al_x$ ($0 \le x \le 20$) alloys.

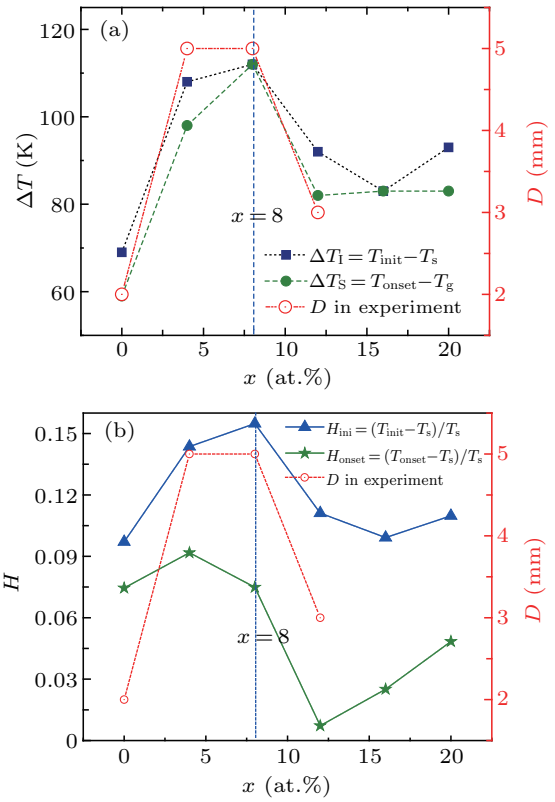



**Fig. 9.** The hereditary supercooled degree $\Delta T$ (a) and the $H$ parameter (b) of [12/555] icosahedra in $(Zr_{50}Cu_{50})_{100-x}Al_x$ alloys during rapid solidification. The open circles are the critical thickness $D$ of $(Zr_{50}Cu_{50})_{100-x}Al_x$ MGs taken from Ref. [7].

## 4. Conclusion

A series of MD simulations is conducted to study the hereditary behavior of clusters in rapidly cooled $(Zr_{50}Cu_{50})_{100-x}Al_x$ melts and its correlation with GFA. LSCA is used to characterize and analyze the 3D local structure units in $(Zr_{50}Cu_{50})_{100-x}Al_x$ alloys. Similar to $Zr_{50}Cu_{50}$ binary MGs, icosahedral clusters play a key role in forming the $(Zr_{50}Cu_{50})_{100-x}Al_x$ ternary MGs. The $f_{\rm LSC}$, $N_{\rm IMRO}$, and $n_{\rm max}$ in MGs at 300 K increase with increasing Al content. By using

inverse tracking, the heredity of [12/555] perfect icosahedra emerges in the $T_l$–$T_g$ supercooled liquids rather than equilibrium melts. With increasing Al atom percentage, either the $T_{onset}$ of continuous heredity or the $T_{init}$ of staged heredity increases monotonously. The $\Delta T_I$ and $\Delta T_S$ of [12/555] icosahedra are closely correlated with the GFA of $(Zr_{50}Cu_{50})_{100-x}Al_x$. A good GFA of Al-doped $Zr_{50}Cu_{50}$ alloy is attributed to the large hereditary supercooled degree of icosahedra. Therefore, the criterion of high heritability of clusters corresponding to good GFA is applicable to the Al-doped $Zr_{50}Cu_{50}$ melts.

## References


[1] Cheng Y Q and Ma E 2011 *Prog. Mater. Sci.* **56** 379
[2] Zhang P, Maldonis J J, Besser M F, Kramer M J and Voyles P M 2016 *Acta Mater.* **109** 103
[3] Kim H K, Lee M, Lee K R and Lee J C 2013 *Acta Mater.* **61** 6597
[4] Inoue A 2000 *Acta Mater.* **48** 279
[5] Kaban I, Jóvári P, Escher B, Tran D T, Svensson G, Webb M A, Regier T Z, Kokotin V, Beuneu B, Gemming T and Eckert J 2015 *Acta Mater.* **100** 369
[6] Cai A, Liu Y, Wu H, Ding D, An W, Zhou G, Luo Y and Peng Y 2015 *Sci. China Mater.* **58** 584
[7] Yu P, Bai H Y, Tang M B, Wang W L and Wang W H 2005 *Acta Phys. Sin.* **54** 3284 (in Chinese)
[8] Xu J, Niu J, Zhang Z, Ge W, Shang C and Wang Y 2016 *JOM* **68** 682
[9] Lozada-Flores O, Figueroa I A, Gonzalez G and Salas-Reyes A E 2018 *Thermochimica Acta* **662** 116
[10] Busch R, Schroers J and Wang W H 2007 *MRS Bull.* **32** 620
[11] Donado R A, Cajahuaring S and Antonelli A 2019 *Phys. Rev. Mater.* **3** 085601
[12] Zhou C, Hu L, Sun Q, Zheng H, Zhang C and Yue Y 2015 *J. Chem. Phys.* **142** 064508
[13] Xu L, Lu Q and Zhang Q 2019 *Mater. Res. Express* **6** 095203
[14] Lekka C E, Bokas G B, Almyras G A, Papageorgiou D G and Evangelakis G A 2012 *J. Alloys Compd.* **536S** S65
[15] Li M Z, Peng H L, Hu Y C, Li F X, Zhang H P, Wang W H 2017 *Chin. Phys. B* **26** 016104
[16] Cheng Y Q, Ma E and Sheng H W 2008 *Appl. Phys. Lett.* **93** 111913
[17] Cheng Y Q, Ma E and Sheng H W 2009 *Phys. Rev. Lett.* **102** 245501
[18] Wen D D, Peng P, Jiang Y Q, Tian Z A, Liu R S and Dong K J 2014 *J. Non-Cryst. Solids* **388** 75
[19] Tian Z A, Liu R S and Dong K J 2011 *Europhys. Lett.* **96** 36001
[20] Deng Y H, Wen D D, Li Y and Peng P 2018 *Philos. Mag.* **20** 1
[21] Plimpton S 1995 *J. Comput. Phys.* **117** 1
[22] Martyna G J, Tobias D J and Klein M L 1994 *J. Chem. Phys.* **101** 4177
[23] Andersen H C 1980 *J. Chem. Phys.* **72** 2384
[24] Zhong L, Wang J W, Sheng H W, Zhang Z and Mao S X 2014 *Nature* **512** 177
[25] Zhang Y, Mattern N and Eckert J 2012 *J. Appl. Phys.* **111** 053520
[26] Wu Z, Mo Y, Lang L, Yu Ai, Xie Q, Liu R and Tian Z 2018 *Phys. Chem. Chem. Phys.* **20** 28088
[27] Kelton K F, Lee G W, Gangopadhyay A K, Hyers R W, Rathz T J, Rogers J R, Robinson M B and Robinson D S 2003 *Phys. Rev. Lett.* **90** 195504
[28] Lan S, Wu Z, Wei X, Zhou J, Lu Z, Neuefeind J and Wang X 2018 *Acta Mater.* **149** 108
[29] Ma D, Stoica A D, Wang X L, Lu Z P, Xu M and Kramer M 2009 *Phys. Rev. B* **80** 014202
[30] Celtek M, Sengul S and Domekeli U 2017 *Intermetallics* **84** 62
[31] Honeycutt J D and Andersen H C 1987 *J. Phys. Chem.* **91** 4950
[32] Wen D D, Peng P, Jiang Y Q, Tian Z A, Li W and Liu R S 2015 *J. Non-Cryst. Solids* **427** 199